A Comparison of Three Ion Sensing Circuits in a Homogeneous Charge Compression Ignition Engine

Article *in* Combustion Science and Technology · February 2017

DOI: 10.1080/00102202.2017.1294587

4 authors, including:

Tung Phan
California Institute of Technology
1 PUBLICATION **1** CITATION
SEE PROFILE

John Hunter Mack
University of Massachusetts Lowell
51 PUBLICATIONS **341** CITATIONS
SEE PROFILE

Robert Dibble
King Abdullah University of Science and Technology
12 PUBLICATIONS **58** CITATIONS
SEE PROFILE

http://dx.doi.org/10.1080/00102202.2017.1294587 Pre-Print

A comparison of three ion sensing circuits in a Homogeneous Charge Compression Ignition engine

Tung M. Phan [1,2,*], J. Hunter Mack [1,3], Ryan H. Butt [1], and Robert W. Dibble [1]

[1] *Department of Mechanical Engineering, University of California at Berkeley, Berkeley, California, United States*
[2] *Present Address: Department of Mechanical and Civil Engineering, California Institute of Technology, Pasadena, California, United States*
[3] *Present Address: Department of Mechanical Engineering, University of Massachusetts Lowell, Lowell, Massachusetts, United States*
***** *Corresponding Author:* California Institute of Technology, MC 104-44, Pasadena, CA 91125, USA. E-mail: tung.phanminh@gmail.com

ABSTRACT

The use of a spark plug ion sensor to detect combustion timing in a Homogeneous Charge Compression Ignition (HCCI) Engine is a technique that could alleviate the need for pressure transducers, a more expensive alternative. One disadvantage of this approach is the difficulty in obtaining a strong signal at lower equivalence ratios. This paper addresses and compares three ion sensing circuitries, namely a voltage follower, a notch filter circuit that removes the 60 Hz wall noise, and a notch filter whose output is coupled to a custom-built "integrator" circuit. The circuit optimizations are aimed at improving signal strength and reliability. The ion signal present in the combustion chamber is experimentally investigated in a 1.9L Volkswagen engine, modified for HCCI operation and fueled with gasoline. Experiments are conducted across different intake temperatures, pressures, and equivalence ratios. It was found that the custom-built circuit provided the best ion signal strength and reliability.

KEYWORDS

HCCI; ion signal; sensor; engine; circuits

REFERENCE

Phan, T. M., Mack, J. H., Butt, R. H., & Dibble, R. W. (2017). A Comparison of Three Ion Sensing Circuits in a Homogeneous Charge Compression Ignition Engine. *Combustion Science and Technology*, 189(8), 1294-1306.

1.0 INTRODUCTION

Homogeneous Charge Compression Ignition (HCCI) is a promising technology that allows for high efficiency and low NOx emission engines. A prominent feature of this engine is the lack of a spark plug or a Diesel fuel injector for control of combustion timing, as premixed HCCI engines rely on autoignition. This creates a problem in precisely determining the combustion timing, a hurdle that must be overcome in order for HCCI to be commercially viable. By exploiting the well-understood phenomenon of ion formation in flames, one can make use of a spark plug based sensor to detect the ions formed from radicals as fuel is burned in the combustion chamber instead of an expensive pressure transducer.

1.1 Homogeneous Charge Compression Ignition

Homogeneous charge compression ignition (HCCI) engines combine characteristics of both diesel and spark-ignited engines, including a homogeneous mixture of fuel and air (similar to a spark-ignited engine) and compression ignition (like a diesel engine). HCCI engines typically operate at lean equivalence ratios ($\phi < 0.4$), producing a low flame temperature (< 2000 K). Therefore oxides of nitrogen (NOx) emissions, which are highly dependent on temperature, are significantly lower compared to traditional combustion methods (Warnatz et al., 1970). Chemical kinetics largely dictate the burn rate and combustion process in HCCI engines, as the temperature rise caused by the compression process is used to produce thermal conditions in which the mixture of fuel and oxidizer autoignite.

A main advantage of HCCI is its ability to achieve efficiencies similar to diesel engines due to high compression ratios, the elimination of throttling losses, and shorter combustion durations (Epping et al., 2002). In addition to the low NOx emissions, HCCI engines also have lower particular matter (PM) emissions in comparison to spark-ignited (SI) and diesel engines. The lean homogeneous air-fuel mixture, and thus the absence of a diffusion flame, contributes to the low PM emissions. Another distinct advantage of HCCI combustion is its ability to operate on a number of different fuels including gasoline (Xiea et al., 2014), diesel (Gray and Ryan, 1997), natural gas (Christensen et al., 1997), ethanol (Maurya and Agarwal, 2011), butanol (Zheng et al., 2015 and Mack et al., 2016), and many different fuel blends (Xingcai et al., 2006, Saisirirat et al., 2011, and Mack et al., 2005).

There are also several challenges facing HCCI. Due to the nature of autoignition, the combustion event is quite rapid and can lead to very high rates of heat and pressure rise at higher equivalence ratios; this results in a high ringing intensity that can damage the engine, lower efficiencies, and increase some emissions. Additionally, since HCCI engines operate at low equivalence ratios, their power output is also limited by the amount of fuel available to the engine. As a result of these limits, HCCI engines tend to have a narrow operating range (Santoso et al., 2005). However, boosted intake pressures (to increase power) (Dec and Yang, 2010), partial fuel stratification (to reduce the pressure rise rate) (Sjöberg et al., 2005), and thermal stratification (Krasselt et al., 2011) are potential avenues to expand the operating range.

Relatively high levels of UHC and CO emissions are another issue for HCCI engines (Christensen et al., 2011 and Oakley et al., 2001), primarily the result of two routes: (1) trapped fuel/air mixture in the crevice regions (Yao, 2009) and (2) cold boundary layers near the chamber surface (Easley, 2001). The gases present in the chamber during the expansion stroke are relatively cold and the temperature is not high enough to fully oxidize the gases exiting the crevice region. In regards to the cold boundary layer, the mixture does not combust in these regions due to thermal quenching.

Lastly, controlling the autoignition event is one of the most difficult problems to solve in HCCI engines, as autoignition is primarily controlled by the chemical kinetics of the mixture. The driving reactions are

very sensitive to the intake temperature and in-cylinder composition. In SI engines, the spark initiates the combustion event; fuel injection timing initiates the combustion event in diesel engines. These methods offer a great deal of control over when combustion occurs. However, in HCCI engines, combustion timing is difficult to control due the autoignition process. In order to control combustion timing, one must accurately measure when the ignition event occurs. Different combustion timing measurement methods have been researched, including microphones (Souder at al., 2004), torque sensors (Taraza et al.,1998), sparkplug ion sensors, and piezo-electric pressure transducers. This study evaluates the use of sparkplug ion sensors as a means of detecting the combustion event.

1.2 Ion Signals in Engines

Ion sensors in engines have been used in a variety of ways, including for misfire and knock detection in SI engines (Auzins et al., 1995, Reinmann et al., 1997, Fan et al., 2012) and flame detectors (Strandh et al., 2003) in HCCI engines. The electrically conductive properties of a flame enable ion measurement since ions are an intermediate step in hydrocarbon combustion processes (Celements and Smy, 1976). A spark plug ion sensor measures the ion signal in the combustion chamber by applying a bias voltage to the sparkplug gap. The ion current signal is produced by ions generated during autoignition; these ions become the conductive carriers within the gap.

The chemi-ionization process shown by Equation 1 drives the ion signal inside an engine (Bogin et al., 2009a). Free electrons are drawn to positively charged center electrode of the sparkplug, thus producing the ion signal which measured by the electric circuitry and providing an indication of combustion event.

$$CH + O \rightarrow CHO^{+} + e^{-} \quad (1)$$

Multiple factors can influence the generation of ions and electrons, and thus the ion signal. Intake pressure, physical location in the combustion chamber, electrode surface area, and fuel composition have all been shown to affect the ion signal (Bogin et al., 2009b and Chen et al., 2013). Of particular interest to this study is the trend that boosted intake pressures suppress the ion signal for neat fuels. Additionally, leaner equivalence ratios result in lower in-cylinder temperatures and lead to decreased production of CH radicals (as seen in Equation 1). This can further reduce the ion signal. At extremely lean conditions, the ion signal becomes indistinguishable from the background noise. Fuel additives have been shown to enhance the strength of the ion signal. Previous studies have shown that the addition of metal acetates improved the ion signal-to-noise ratio at naturally aspirated and boosted intake conditions (Butt et al., 2015 and Mack et al., 2016).

2.0 EXPERIMENTAL SET-UP

2.1 Engine Specifications

The engine used in the experimental portion of this paper is a modified four-cylinder 1.9 L Volkswagen TDI engine. The engine specifications and operating conditions are listed in Table 1. In order to operate in a HCCI mode, the engine includes significant modifications: replacement of the stock deep-bowl pistons with relatively flat pistons to reduce heat transfer, modification of the glow plug holes to fit standard 10 mm spark plugs (the ion sensors), installation of in-cylinder quartz piezoelectric pressure transducers (AVL Model QH33D) in the direct fuel injector ports, design of a custom injection control

system using solid-state relays and control signals generated from a National Instruments LabView program, use of a custom intake manifold including a port fuel injector system, monitoring of exhaust composition via wide-band lambda sensors, isolation of the cylinder 4 exhaust manifold to ensure accurate measurement of the equivalence ratio, replacing the turbocharger with an external 100 HP compressor (including a 6 m^3 surge tank) to achieve boosted intake conditions, measurement of intake pressure via a piezoresistive pressure sensor (Kulite XTEL 190M) at a crank-angle resolution, and temperature monitoring via multiple K-type thermocouples in the intake and exhaust manifolds.

Table 1. Engine specifications and operating conditions.

Configuration	4 cylinder
Displacement	1.9 L
Compression ratio	17.0 : 1
Bore	79.5 mm
Stroke	95.5 mm
Connection rod length	144.0 mm
Fuel injection	Port fuel injection
Fuel pressure	45 PSI
Valves (intake, exhaust)	1, 1
Intake valve open (IVO)	2 ^{o}CA bTDC
Intake valve close (IVC)	47.5 ^{o}CA aBDC
Exhaust valve open (EVO)	47.5 ^{o}CA bBDC
Exhaust valve close (EVC)	8 ^{o}CA aTDC
Overlap	0 ^{o}CA
Maximum valve lift	10 mm
Engine speed	1800 RPM
Volume BDC	504.72 cm^3
Volume TDC	29.69 cm^3

Engine speed is controlled with an alternating current (AC) motor-generator connected to the engine using a direct-drive shaft and clutch. The engine speed is maintained at a constant 1800 rpm. Figure 1 shows a schematic of the HCCI engine test bench and key sensors for the data acquisition and control. The engine has been converted to single-cylinder operation by deactivating cylinders 1,2, and 3. The configuration of the engine facility and data acquisition is similar to previous studies (Butt et al., 2015 and Vuilleumier et al., 2013).

[Figure 1]

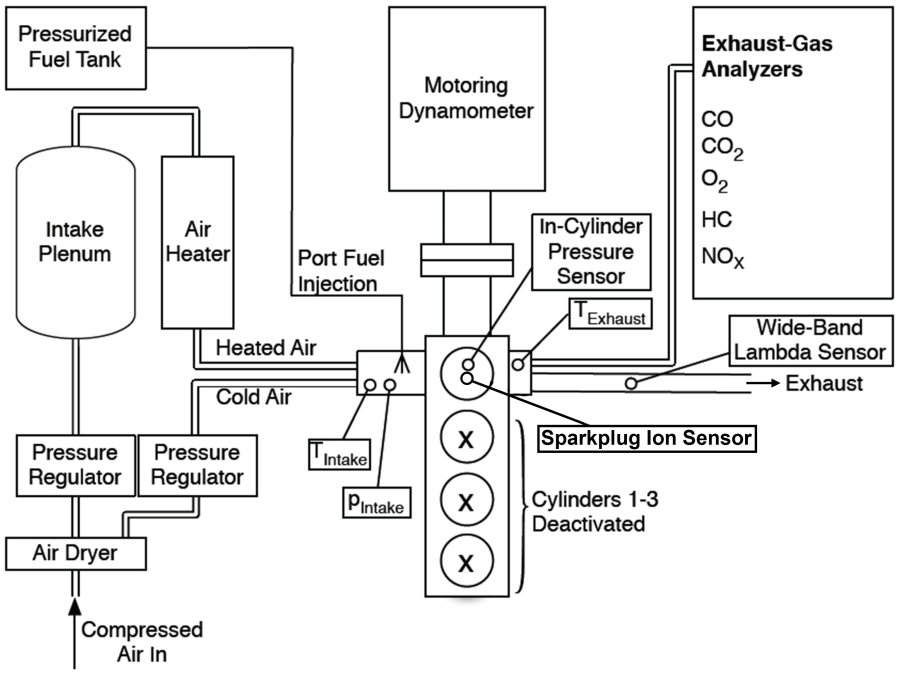

Figure 1. Schematic of HCCI engine test bench, including intake system, and key diagnostic sensors.

In-cylinder pressure is monitored using a pressure transducer connected to a charge amplifier. The pressure measurements are triggered by a crankshaft encoder with a resolution of 4 samples per crank angle degree. At each testing condition, 300 consecutive thermodynamic cycles are measured and recorded. The pressure data is used to calculate the heat release rate and indicated mean effective pressure. The most important recorded parameters for the controlling of the engine and the evaluation include intake pressure (p_{intake}), intake temperature (T_{intake}), in-cylinder pressure ($p_{in\text{-}cylinder}$), equivalence ratio (Φ), exhaust temperature ($T_{exhaust}$), coolant temperature ($T_{coolant}$), and oil temperature (T_{oil}). The coolant and oil temperature are kept in a constant range to guarantee comparable results during operation of the engine.

Fuel is port-injected in the intake manifold of cylinder 4 after mixing of the hot and cold air streams. The fuel injector is connected to a 12-volt battery through a solid-state relay, which provides control of the amount of fuel injected by varying the pulse width. The equivalence ratio is measured using wideband lambda sensors (Innovate Motorsports LC-1), located in the exhaust manifold of cylinder 4. The lambda sensors output an analog voltage proportional to the oxygen (or unburned fuel fraction) in the exhaust. The lambda sensor output is used to control the pulse width of the fuel injection event by a feedback control loop.

The crank angle at which 50% of the heat from combustion has been released (CA50) is calculated from the in-cylinder pressure data and monitored in real-time during testing. CA50 serves as a feedback parameter for adjusting the intake temperature T_{intake}, which is controlled by intake air heater. Combustion timing is advanced as the intake temperature is increased. As shown in Figure 1, the intake temperature is fine-tuned by adjusting the amount of mass flow of hot air and cold (ambient temperature) air. The amount of cold air is regulated via the pressure regulator installed upstream of the intake in the cold air supply.

2.2 Ion Circuits

The primary ion sensing circuit consists of a 237 V battery providing a bias voltage for a spark plug in series with a 241 kΩ resistor. With the presence of ions in the spark plug, a current is drawn through the resistor, and the resultant voltage drop is fed to a National Instruments LabView program for analysis. Various secondary filter and amplifier circuits are implemented and tested using TL082 operational amplifiers powered by a 25 V bench supply source. Among these are a unity gain circuit, a 60 Hz notch filter, and a custom-built integrator whose input is connected to the output of a 60 Hz notch filter and whose output signal is passed through a high-pass filter.

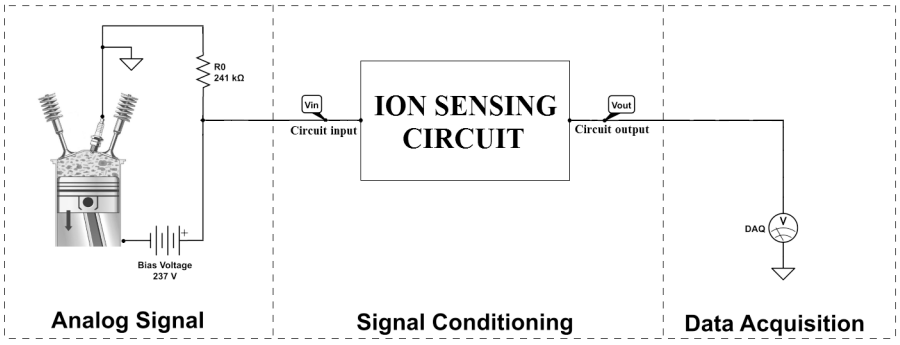

Figure 2. Experimental setup.

As the fuel-air mixture autoignites in the combustion chamber, an ion current is formed across the two biased electrodes of a spark plug, which acts like a capacitor. The bias voltage for the spark plug is 237 V. The ion current signal is converted to a voltage signal (V_{in}) via a voltage drop across a 241 kΩ resistor. The input signal (V_{in}) from the engine side is passed into a circuit for signal processing before reappearing as V_{out} on the DAQ side. The filtered ion voltage signal (V_{out}) is sent to the NI DAQ system for data logging as shown in Figure 2.

The notch filter and integrator circuit is shown in Figure 3. The output of the 60 Hz wall noise active notch filter sends the filtered ion signal to the input of an integrator whose time constant was experimentally determined based on the engine RPM. The integrator circuit adds up the collected charge formed over about 20 CAD to generate a pulse (preamp signal) that is further passed onto a final circuitry (high pass filter) that attenuates low frequency noise.

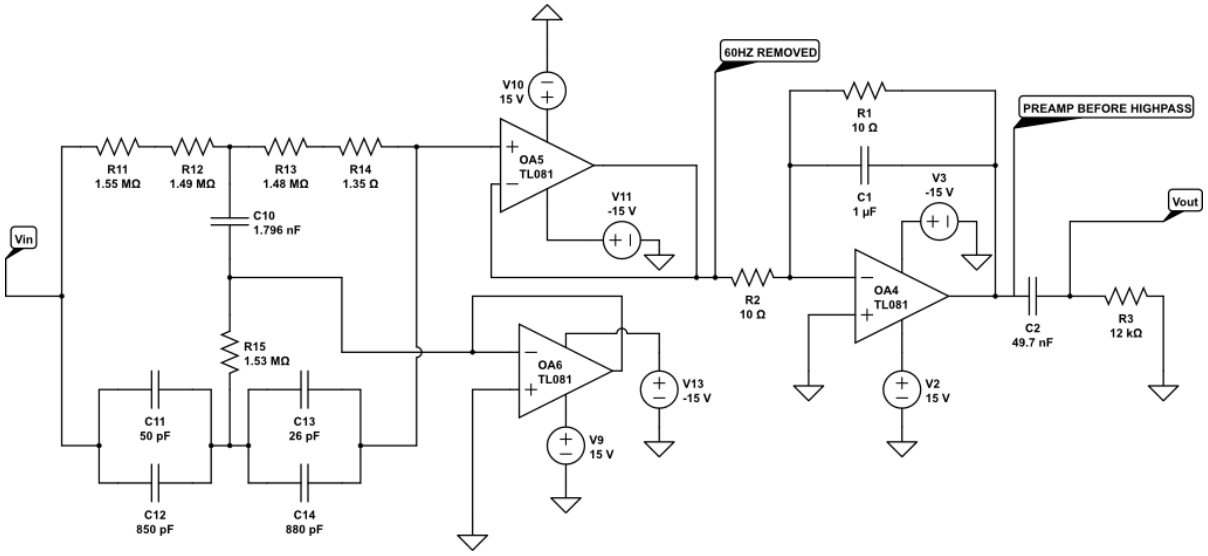

Figure 3. Notch filter and integrator circuit.

The notch filter circuit is shown in Figure 4. An active twin-T notch filter with a roll-off rate of 40 db/decade is used to remove 60 Hz noise from the voltage signal. This circuit also doubles as an isolation circuit separating the input side (raw signal from the combustion chamber) from the output side of the circuit, thus protecting the data acquisition system from possible voltage spikes. The resonance frequency of the circuit is 60.3 Hz. Four capacitors are installed as close as possible to the operational amplifier's power supply pins on the breadboard for AC noise reduction.

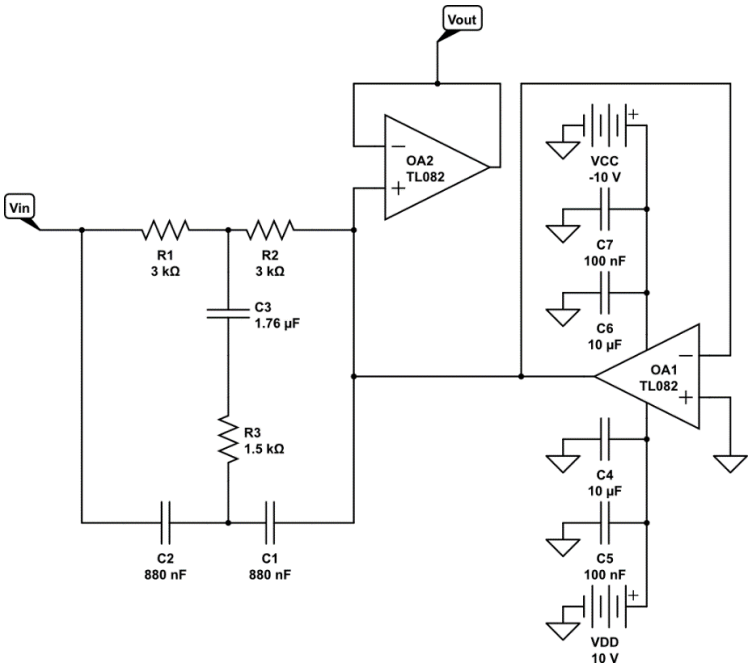

Figure 4. Notch filter.

The unity gain circuit is shown in Figure 5. The right side operational amplifier is part of the unity gain circuit which simply "replicates" the raw ion signal. The second op amp is connected as shown to 4 capacitors to minimize noise originating from the power supply.

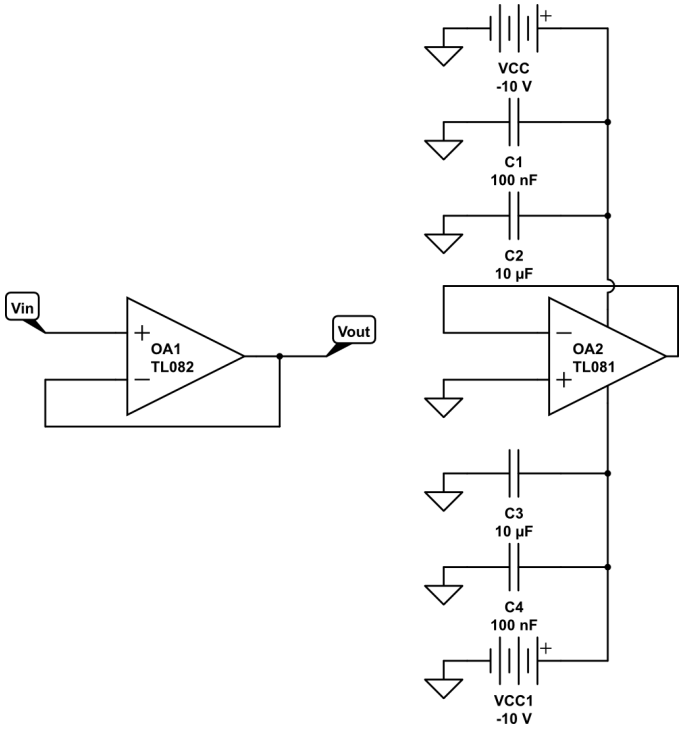

Figure 5. Unity gain circuit.

2.3 Test Procedures

The engine was operated at a constant speed of 1800 RPM. The intake temperature was adjusted for desired crank angle degree CA50. A reference equivalence ratio (φ) is controlled by the fuel injection pulse width. Exhaust data were also recorded for determining the precise equivalence ratio. To ensure that the testing/engine conditions were as close to one another as possible for the three circuits, data were collected for each test point (corresponding to one CA50 and one φ) with the three circuits switched in and out in succession. Data for each test point is recorded three times over 300 consecutive engine cycles each, yielding a total of 900 cycles per test point for improved statistics. CA50 values range from 0 to 8 in 2-degree increments. The values over 900 cycles are averaged and presented in the data section.

3.0 RESULTS

Pressure and ion traces were captured across a range of combustion timings (CA50) for each of the individual circuits. Figure 6 shows a comparison of the pressure and ion traces for the integrator (A), notch (B), and unity (C) filters respectively obtained for an equivalence ratio of 0.16. The integrator circuit provided the largest ion signal, followed by the unity and notch circuits. A maximum ion signal of

25.9 μA was observed with the integrator circuit, which corresponded to the earliest CA50 (see also Figure 7). With the exceptions of CA50 = 2 for the integrator circuit and CA50 = 0 for the notch and unity circuits, as CA50 is retarded, the ion signal decreases.

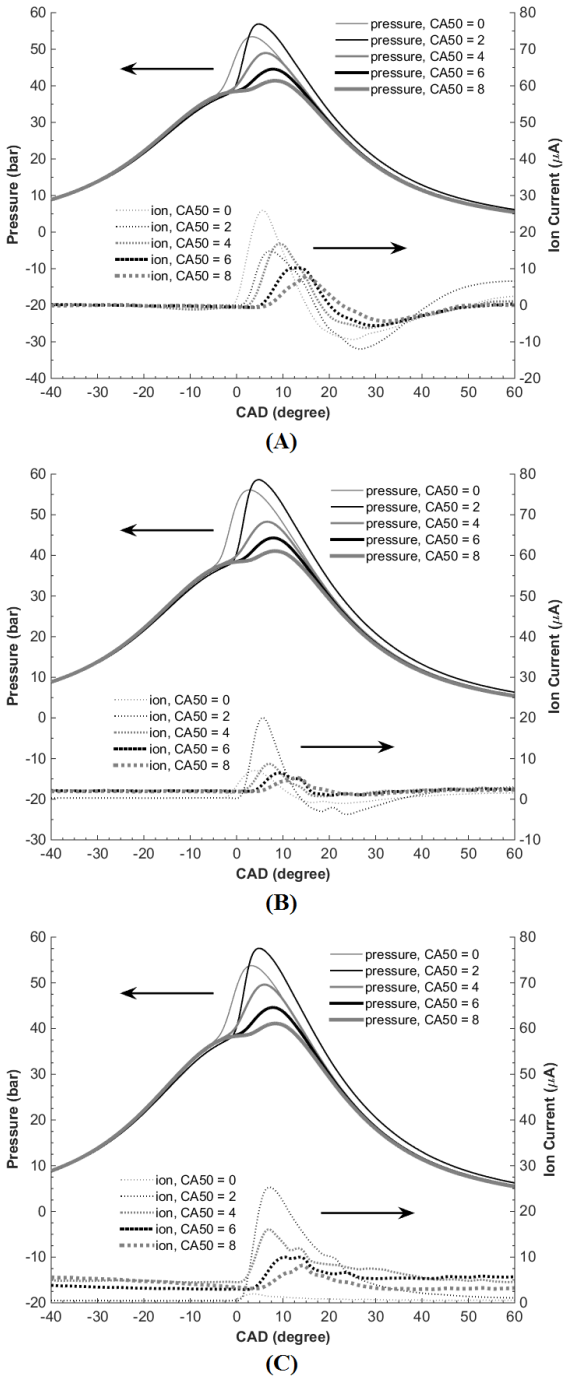

Figure 6. Pressure and ion signal versus CA50 at φ = 0.16 for the (A) integrator circuit, (B) notch circuit, and (C) unity circuit.

As a means of comparing the ion signal for each of the circuits, Figure 7 shows the ion signal with a constant CA50 at TDC and an equivalence ratio of 0.16 for the integrator, notch, and unity circuits. This shows the general trend in which the amplitude of the signal increases going from the unity gain circuit to the notch and finally the integrator circuit. Secondary peaks can also be seen in the ion traces corresponding to the integrator and the notch circuits.

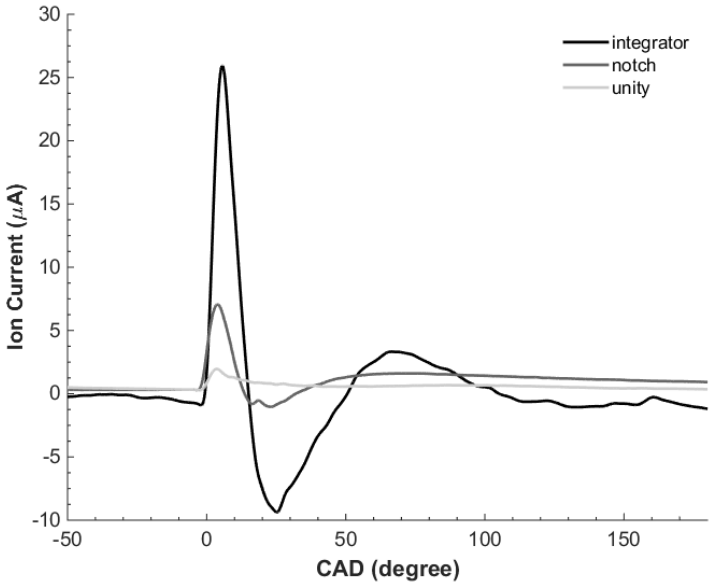

Figure 7. Ion traces at CA50 = 0 and φ = 0.16 for all circuits

In addition to the peak ion signal, another important metric is the signal to noise ratio, which is defined as the average power of the signal to that of the noise. Specifically,

$$SNR = \frac{P_{signal}}{P_{noise}} \tag{2}$$

where P represents the power averaged over a period T.

$$P = \frac{1}{T}\int_0^T I^2 dt \tag{3}$$

Figure 8 (A) compares the SNR for each of the circuits over a range of combustion timings. The notch and integrator circuits provide the highest SNR, while the unity circuit is by far inferior.

To further characterize and assess the circuits' relative performance and their signals, we introduce a metric that is named stability for convenience. This is defined to be the ratio of the mean standard deviation of the noise to the mean standard deviation of the signal. Figure 8 (B) reveals that the integrator circuit generally provides a desirably high stability ratio, while the notch and unity filters are generally slightly lower.

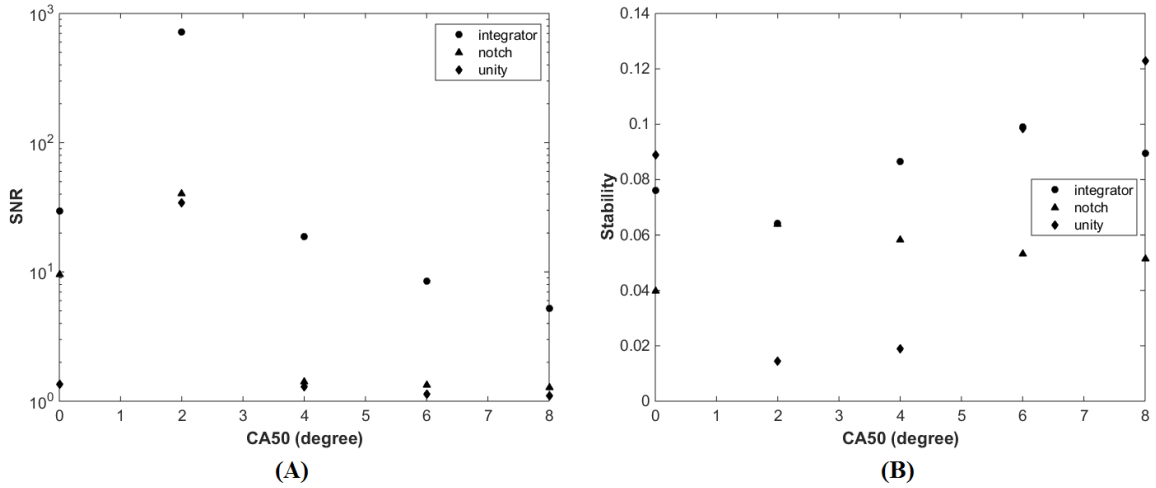

Figure 8. (A) Signal-to-noise ratio versus CA50 for all circuits at φ = 0.16. (B) Stability (ratio of mean standard deviation of the ion signal to the mean standard deviation of noise) versus CA50 for all circuits at φ = 0.16.

A delay between combustion timing (CA50) and peak ion signal can complicate control strategies. Therefore, minimizing the delay is an important task for any circuit design. Table 2 lists the delay for each circuit at each CA50 operating point. The negative delays in the notch and unity ion traces for φ = 0.13 at CA50 = 0 are somewhat surprising and are possibly associated with the spark plug reaching its detecting limits for ions at low concentrations.

[Table 2]

Table 2. Delay between peak of ion signal and CA50 for all circuits.

	CA50				
Circuit (ϕ)	0	2	4	6	8
Integrator (0.16)	2.25	2.5	3	5.25	7
Notch (0.16)	1.25	1	0.5	1.25	4.25
Unity (0.16)	0.25	2.5	1	2.75	6
Integrator (0.13)	2	3.5	-	-	-
Notch (0.13)	-0.25	1	1.75	7	-
Unity (0.13)	-0.25	1.5	-	-	-

Table 3 summarizes the results and compares all three circuits tested in this study. Each of the circuits has distinct advantages and disadvantages. Two interesting features observed in the ion traces are peak clamping and secondary peaks. Peak clamping is a phenomenon related to stability where the ion speak appears fixed over time during steady state operation of the engine. This is clearly a desirable feature contributing to the stability of the ion trace. Secondary peaks are the result of delayed discharges of capacitive elements used in the construction of the notch and integrator circuits. These peaks can

introduce confounding features to the corresponding ion traces making interpretation and comparison to the respective pressure traces more challenging. Fortunately, the peaks are these signals are generally smaller than the main peak ion signals, allowing in most cases for easy differentiation.

Table 3. Summary of discussion

Circuit	Advantages	Disadvantages	Comments
Integrator circuit	Highest stability; Good signal strength	Relatively large time delay.	Peaks are usually clamped (remains stationary); secondary peaks due to discharge from capacitor
Notch filter	Semi-stable; Small delay; Good signal strength	Greatly attenuated at high CAD and low ϕ	Peaks not clamped; Small secondary peaks
Unity gain	Simple to implement; small delay	Very unstable and noisy	Peaks not clamped; No secondary peaks

4.0 CONCLUSIONS

All of the tested ion sensing circuits are capable of predicting the combustion event in good agreement with signals from the pressure transducer when the fuel-air equivalence ratio is approximately 0.16 and above. Below this level, either the noise signal overwhelms the ion signal or not enough ions are formed in the vicinity of the spark plug in order for an easy-to-detect ion current to pass through the resistor. The notch filter was able to detect ion signals at the lower equivalence ratios, yet the peak signal is greatly attenuated. The custom-built integrator circuit produces the highest peak ion signal and is the most stable but also has the largest time delay. The unity circuit, while the simplest to implement and having no time delay, performed worst across all other metrics. With these three simple circuits, we have therefore been able to demonstrate that there is still room for optimizing ion detection from the circuitry side. For future work, we would like to continue experimenting with circuit designs with an aim to eventually develop a more complete theory and systematic procedure that can supersede the current ad hoc approach.

REFERENCES

Auzins, J., Johansson, H., and Nytomt, J. (1995) Ion-gap sense in misfire detection, knock and engine control. SAE Technical Paper 950004.

Bogin, G.E., Mack, J.H., and Dibble, R.W. (2009a). Spark Plug Modifications for Improving Ion Sensing Capabilities in a Homogeneous Charge Compression Ignition (HCCI) Engine. Proceedings of the ASME ICE Spring Conference, ICES2009-76161.

Bogin, G.E., Mack, J.H., and Dibble, R.W. (2009b). Fuel effects of ion sensing in a homogeneous charge compression ignition (HCCI) engine.SAE Technical Paper 2009-01-1805.

Butt, R.H., Chen, Y., Mack, J.H., Saxena, S., Dibble, R.W., and Chen, J.Y. (2015). Improving ion current of sparkplug ion sensors in HCCI combustion using sodium, potassium, and cesium acetates:

Experimental and numerical modeling. Proceedings of the Combustion Institute, Volume 35, Issue 3.

Celements, R.M., and Smy, P.R. (1976). The variation of ionization with air/fuel ratio for a spark ignition engine. J. Applied Physics, Vol 47(2).

Chen, Y., Li, L., Miao, Q., Cao, Y., Liu, Y., Liu, Z., and Deng, J. (2013). Effect of Stratification on Ion Distribution in HCCI Combustion Using 3D-CFD with Detailed Chemistry. SAE Technical Paper 2013-01-2512.

Christensen, M., Johansson, B., and Einewall, P. (1997). Homogeneous Charge Compression Ignition (HCCI) Using Isooctane, Ethanol and Natural Gas - A Comparison with Spark Ignition Operation. SAE Technical Paper 972874.

Christensen, E., Yanowitz, J., Ratcliff, M., and McCormick, R.L. (2011). Renewable Oxygenate Blending Effects on Gasoline Properties. Energy & Fuels, Vol. 25, pp. 4723–4733.

Dec, J., and Yang, Y. (2010). Boosted HCCI for High Power without Engine Knock and with Ultra-Low NOx Emissions - using Conventional Gasoline. SAE Int. J. Engines 3(1), pp. 750-767.

Easley, W.L., Agarwal, A., and Lavoie, G.A. (2001). Modeling of HCCI Combustion and Emissions Using Detailed Chemistry. SAE Technical Paper 2001-01-1029.

Epping, K., Aceves, S., Bechtold, R., and Dec, J. (2002). The Potential of HCCI Combustion for High Efficiency and Low Emissions. SAE Technical Paper 2002-01-1923.

Fan, Q., Bian, J., Lu, H., Tong, S., and Li, L. (2012). Misfire Detection and Re-ignition Control by Ion Current Signal Feedback during Cold Start in Two-stage Direct-Injection Engines. Int. Journal of Eng. Research, Vol 15(1), pp. 37–47.

Gray, A.W., and Ryan, T.W. (1997). "Homogeneous Charge Compression Ignition (HCCI) of Diesel Fuel," SAE Technical Paper 971676.

Krasselt, J., Foster, D., Ghandhi, J., Herold, R., Reuss, D., and Najt, P. (2009). Investigations into the Effects of Thermal and Compositional Stratification on HCCI Combustion – Part I: Metal Engine Results. SAE Technical Paper 2009-01-1105.

Mack, J.H., Schuler, D., Butt, R.H., and Dibble, R.W. (2016). Experimental investigation of butanol isomer combustion in Homogeneous Charge Compression Ignition (HCCI) engines. Applied Energy, Vol 165, pp. 612-626.

Mack, J.H., Butt, R.H., Chen, Y., Chen, J.Y., and Dibble, R.W. (2016). Experimental and numerical investigation of ion signals in boosted HCCI combustion using cesium and potassium acetate additives. Energy Conversion and Management, Volume 108, pp. 181-189.

Mack, J.H., Flowers, D.L., Buchholz, B.A., and Dibble, R.W. (2005). The Effect of the Di-Tertiary Butyl Peroxide (DTBP) additive on HCCI Combustion of Fuel Blends of Ethanol and Diethyl Ether. SAE Technical Paper 2005-01-2135.

Maurya, R.K., and Agarwal, A.K. (2011). Experimental study of combustion and emission characteristics of ethanol fuelled port injected homogeneous charge compression ignition (HCCI) combustion engine. Applied Energy, Volume 88, Issue 4, pp. 1169-1180.

Oakley, A., Zhao, H., Ladommatos, N., and Ma, T. (2001). Experimental Studies on Controlled Autoignition (CAI) Combustion of Gasoline in a 4-Stroke Engine. SAE Technical Paper 2001-01-1030.

Reinmann, R., Saitzkoff, A., and Mauss, F. (1997). In-Cylinder Pressure Measurement using the Spark Plug as an Ionization Sensor. SAE Technical Paper 970857.

Saisirirat, P., Togbé, C., Chanchaona, S., Foucher, F., Mounaim-Rousselle, C., and Dagaut, P. (2011). Auto-ignition and combustion characteristics in HCCI and JSR using 1-butanol/n-heptane and ethanol/n-heptane blends, Proceedings of the Combustion Institute, Volume 33, Issue 2, pp. 3007-3014.

Santoso, H., Matthews, J., and Cheng, W.K. (2005). Managing SI/HCCI Dual-Mode Engine Operation. SAE Technical Paper 2005-01-0162.

Sjöberg, M., Dec, J., and Cernansky, N. (2005). Potential of Thermal Stratification and Combustion Retard for Reducing Pressure-Rise Rates in HCCI Engines, Based on Multi-Zone Modeling and Experiments. SAE Technical Paper 2005-01-0113.

Souder, J.S., Mack, J.H., Hedrick, J.K., and Dibble, R.W. (2004). Microphones and knock sensors for feedback control of HCCI engines. ASME ICEF2004-960.

Strandh, P., Christensen, M., Bengtsson, J., Johansson, R., Vressner, A., Tunestal, P., and Johansson, B. (2003). Ion current sensing for HCCI combustion feedback. SAE Technical Paper 2003-01-3216.

Taraza, D., Henein, N.A., and Bryzik, W. (1998). Determination of the Gas Pressure Torque of a Multicylinder Engine from Measurements of the Crankshaft's Speed Variation. SAE Technical Paper 980164.

Vuilleumier, D., Selim, H., Dibble, R.W., and Sarathy, M. (2013) Exploration of Heat Release in a Homogeneous Charge Compression Ignition Engine with Primary Reference Fuels. SAE Technical Paper 2013-01-2622.

Warnatz, J., Maas, U., and Dibble, R.W. (2006). Combustion. Physical and chemical fundamentals, modeling and simulation, experiments, pollutant formation. Springer, 4th ed.

Xiea, H., Lia, L., Chena, T., and Zhao, H. (2014). Investigation on gasoline homogeneous charge compression ignition (HCCI) combustion implemented by residual gas trapping combined with intake preheating through waste heat recovery. Energy Conversion and Management, Volume 86, pp. 8-19.

Xingcai, L., Yuchun, H., Libin, J., Linlin, Z., and Zhen, H. (2006). Heat Release Analysis on Combustion and Parametric Study on Emissions of HCCI Engines Fueled with 2-Propanol/n-Heptane Blend Fuels. Energy & Fuels 20(5), pp. 1870-1878.

Yao, M., Zheng, Z., and Liu, H. (2009). Progress and recent trends in homogeneous charge compression ignition (HCCI) engines. Progress in Energy and Combustion Science, vol. 35, pp. 398–437.

Zheng, M, Han, X, Asad, U, and Wang, J. (2015). Investigation of butanol-fuelled HCCI combustion on a high efficiency diesel engine, Energy Conversion and Management 98; pp. 215–224.